Received: 6 January 2020 | Revised: 27 July 2020 | Accepted: 29 July 2020 | Published on: 14 September 2020

DOI: 10.1002/qj.3885

Quarterly Journal of the Royal Meteorological Society RMetS

RESEARCH ARTICLE

# Improving the ocean and atmosphere in a coupled ocean–atmosphere model by assimilating satellite sea-surface temperature and subsurface profile data

Qi Tang | Longjiang Mu | Dmitry Sidorenko | Helge Goessling | Tido Semmler | Lars Nerger

Alfred Wegener Institute, Helmholtz Centre for Polar and Marine Research, Bremerhaven, Germany

**Correspondence**
Qi Tang, Alfred Wegener Institute, Helmholtz Centre for Polar and Marine Research, Bremerhaven, Germany.
Email: qi.tang@awi.de

**Funding information**
Bundesministerium für Bildung und Forschung, Grant/Award Number: 01LN1701A; Earth System Modelling Project (ESM); Open access funding enabled and organized by Projekt DEAL.

**Abstract**

An ensemble-based data assimilation framework for a coupled ocean–atmosphere model is applied to investigate the influence of assimilating different types of ocean observations on the ocean and atmosphere simulation. The data assimilation is performed with the parallel data assimilation framework (PDAF) for the climate model AWI-CM. Observations of the ocean, namely satellite sea-surface temperature (SST) and temperature and salinity profiles, are assimilated into the ocean component. The atmospheric state is only influenced by the model dynamics. Different assimilation scenarios were carried out with different combinations of observations to investigate to what extent the assimilation into the coupled model leads to a better estimation of the state of the ocean as well as the atmosphere. The influence of the data assimilation is assessed by comparing the ocean prediction with dependent and independent ocean observations. For the atmosphere, the assimilation result is compared with the ERA-Interim atmospheric reanalysis data. The ocean temperature and salinity are improved by all the assimilation scenarios in the coupled system. The assimilation leads to a response of the atmosphere throughout the troposphere and impacts the global atmospheric circulation. Globally the temperature and wind speed are improved in the atmosphere on average.

**KEYWORDS**

coupled model, data assimilation, sea-surface temperature, temperature and salinity profiles

## 1 | INTRODUCTION

Traditionally, different components of the Earth system such as the ocean and the atmosphere are simulated by separate models with influences of other components being modelled as boundary conditions or forcings. However, the oceans and the atmosphere are connected and interact with each other. A consistent initial condition for these different components is required and is expected to provide a better forecast for both the ocean and the atmosphere. Earth system models simulate different components like the ocean, atmosphere, sea ice and land

surface and their interactions in one framework including fluxes in between them which can thus lead to more consistent simulations than standalone models. Such models can capture the key physical processes for each of the coupled components and can help to better understand the impact of changes in one component on other components (Miller *et al.*, 2017). However, when using a coupled Earth system model, it can only represent a climatological state, but not the current weather conditions unless one uses data assimilation (DA) to initialize the model forecasts.

DA combines the model state with real-world observations and thus provides an optimized state estimate of the coupled model. After a certain period with data assimilation, the state estimate can be close enough to the reality, and can then be used to initialize a new prediction simulation. The common approach used is the weakly coupled DA, which means that the assimilation acts separately on each component in the coupled model (Penny and Hamill, 2017). Thus, observations of one component only directly influence their own component. The other components can benefit from the DA through the model dynamics. One example is given by Laloyaux *et al.* (2016) who assimilated temperature and salinity observations into the ocean model using the three-dimensional variation (3D-Var) method and air temperature, surface pressure and wind velocity into the atmosphere with the 4D-Var method. Their results showed that the assimilation into one model affected the other model states, especially for the upper ocean and lower atmosphere temperature. Another example is by Liu *et al.* (2013), who found that assimilating atmospheric observations into a coupled ocean–atmosphere model was important for the estimation of not only the atmospheric but also the oceanic variables in the mid-latitudes. Moreover, assimilating only atmospheric observations into the atmosphere model in a coupled ocean–atmosphere system can better reproduce the intensity change of a typhoon (Kunii *et al.*, 2017). Compared to the uncoupled analysis, the weakly coupled ocean–atmosphere assimilation system provided an improved forecast for both the atmosphere and the ocean (especially for the sea-surface temperaure prediction) by applying DA into both the ocean and the atmosphere (Browne *et al.*, 2019; Guiavarc'h *et al.*, 2019; Skachko *et al.*, 2019). Besides, climate variabilities were well simulated (Karspeck *et al.*, 2018) and most of the biases were corrected (Chang *et al.*, 2013) by such a coupled DA system. Other benefits of coupled DA systems include better reconstruction of the ocean heat content variability and trends (Zhang *et al.*, 2007) and better ocean and atmosphere forecasts from seasonal to interannual time-scales (Sugiura *et al.*, 2008). However, Lea *et al.* (2015) found assimilation into both the ocean and the atmosphere in a coupled system gave similar analysis states compared to assimilation into the separate ocean and atmosphere alone models.

To the authors' knowledge, until now no studies assimilated only the ocean observations into the ocean component in a coupled ocean–atmosphere model and explored their influence on the atmospheric variables of the atmosphere component for real-world experiments using the Ensemble Kalman Filter (EnKF). In this study, we investigate whether DA can improve the prediction of the ocean as well as the atmospheric state by assimilating multiple types of ocean observations into the ocean component in a coupled ocean–atmosphere model. These assimilation experiments were designed to answer the following questions: (a) What is the assimilation effect on the ocean in this coupled system? (b) What is the effect of the different observational types sea-surface temperature (SST) and subsurface profiles? and (c) What is the impact of the assimilation of ocean variables on the atmospheric state?

The article is structured as follows. Section 2 briefly describes the coupled ocean–atmosphere model and the data assimilation method we used for the numerical experiments. Section 3 provides the configuration and input for the data assimilation experiments. Section 4 discusses the data assimilation results and Section 5 the conclusion of this study.

## 2 | DESCRIPTION OF THE COUPLED DATA ASSIMILATION SYSTEM

### 2.1 | The coupled ocean–atmosphere model: AWI-CM

The AWI (**A**lfred **W**egener **I**nstitute) climate model (AWI-CM: Sidorenko *et al.*, 2015) is used as the coupled ocean–atmosphere model to simulate the global ocean as well as the atmosphere circulation and their interactions. AWI-CM consists of the finite element sea ice–ocean model (FESOM v1.4: Wang *et al.*, 2014) coupled with the atmosphere model ECMWF HAMberg version (ECHAM6: Stevens *et al.*, 2013) using the coupler software OASIS3-MCT (Model Coupling Toolkit) (Valcke *et al.*, 2013). FESOM is a global ocean general circulation model implementing unstructured mesh, which allows varying resolutions within the model domain. The advantage of unstructured meshes for ocean modelling is described by Danilov (2013). ECHAM6 is a spectral-based atmospheric general circulation model integrated with the land vegetation model JSBACH. It mainly serves as the atmospheric component of the Max Planck Institute Earth System Model (MPI-ESM) which allows e.g. predicting seasonal surface temperature (Baehr *et al.*, 2015),

or investigating the impact of regional cloud changes (Voigt and Shaw, 2016). With ensemble data assimilation, MPI-ESM was used, for example, by Brune *et al.* (2015). A detailed description of AWI-CM is given by Sidorenko *et al.* (2015) and Rackow *et al.* (2018). It has been applied to investigate the impact of ocean and atmosphere model resolution on Arctic sea ice and Atlantic Ocean heat transport (Docquier *et al.*, 2019), the circulation of the North Atlantic Ocean (Sein *et al.*, 2018), the potential sea ice predictability with ensemble experiments (Juricke *et al.*, 2014), the predictability of the Arctic sea ice edge (Goessling *et al.*, 2016) and the seasonal atmospheric responses to reduced Arctic sea ice (Semmler *et al.*, 2016).

### 2.2 | Data assimilation method: Local error subspace transform Kalman filter

The data assimilation method we used here is the local error subspace transform Kalman filter (LESTKF: Nerger *et al.*, 2012b) that is implemented in the software Parallel Data Assimilation Framework (PDAF, http://pdaf.awi.de: Nerger *et al.*, 2005; Nerger and Hiller, 2013). Like in all EnKFs, the model uncertainties are represented by an ensemble of realizations of model states, each represented by a state vector. The state vector can include multiple variables from either one component or different components in the coupled physical system. In this study all the ocean variables including sea-surface height, ocean temperature, salinity and velocity in three directions are part of the state vector, while the atmospheric variables are not treated as a state vector of the update. At a time step $t$, the ensemble of state vectors is propagated from the previous time-step $t-1$ by applying the model dynamic equations, which is called the forecast phase. Once observations are available, the ensemble states are updated by combining the observations with the model forecast. This is called the analysis step. The weight matrix for the observational influence is calculated based on the covariance matrix of the forecast ensemble and the observation error and it gives the relative weight to the forecast and the observations. Once the analysis is done, the updated ensemble of state vectors will be used as the input for the next forecast phase.

Covariance inflation (Anderson and Anderson, 1999) and localization (Hamill *et al.*, 2001; Houtekamer and Mitchell, 2001) are two commonly used methods to improve the filter performance of EnKFs. The effect of inflation is to increase the ensemble variance, thus avoiding filter convergence. Localization can reduce the spurious errors in the ensemble-estimated covariance matrix caused by a small number of samples. In this study, domain localization and observation localization are used (Nerger *et al.*, 2012a). For a given location in the model grid only observations within a prescribed localization radius are taken into account. The LESTKF calculates an ensemble transform matrix in the local error subspace. This makes the computation more efficient compared to the original EnKF with local analysis (Evensen, 2003).

As an open-source software framework, PDAF provides fully implemented and parallelized ensemble filter algorithms as well as support for the parallel ensemble integrations. It has been used for DA with small models as well as with high-dimensional models on supercomputers (e.g. Yang *et al.*, 2015; Kurtz *et al.*, 2016; Mu *et al.*, 2018; Androsov *et al.*, 2019). The coupling of PDAF with AWI-CM is described in Nerger *et al.* (2019). The current configuration can perform weakly coupled data assimilation, i.e. assimilating the ocean observations into the ocean component of the coupled AWI-CM model. The atmospheric variables are not directly updated via the covariance matrix but indirectly influenced by the model dynamics in this weakly coupled data assimilation.

## 3 | NUMERICAL EXPERIMENTS WITH AWI-CM-PDAF

### 3.1 | Model set-up

The set-up of the AWI-CM model we used in this study follows that used in Sidorenko *et al.* (2015). In the ocean model FESOM, we use a varying horizontal resolution between 25 km in the tropical and northern North Atlantic regions and 150 km in the open ocean, which is called "CORE II" mesh (Large and Yeager, 2009; Wang *et al.*, 2014). In the vertical direction 47 layers are used with different thicknesses, varying from 10 to 250 m from top to bottom. In the atmospheric model ECHAM6, we use the resolution T63, corresponding to a horizontal resolution of 1.875°. In the vertical direction, the model is divided into 47 sigma-layers. The time steps for FESOM and ECHAM are 900 and 400 s, respectively. The coupling frequency is set to 1 hr.

### 3.2 | Model initialization

Prior to the data assimilation, a serial long-term historical simulation from the year 1950 to the end of 2015 was carried out as a spin-up run to obtain the suitable initial state for the ocean and the atmosphere as well as the exchange fluxes between the two components (Haarsma *et al.*, 2016; Docquier *et al.*, 2019). For the ocean component, an initial ensemble of the model state is generated using the second-order exact sampling method (Pham *et al.*, 1998). First, a one-year simulation with AWI-CM was run for the

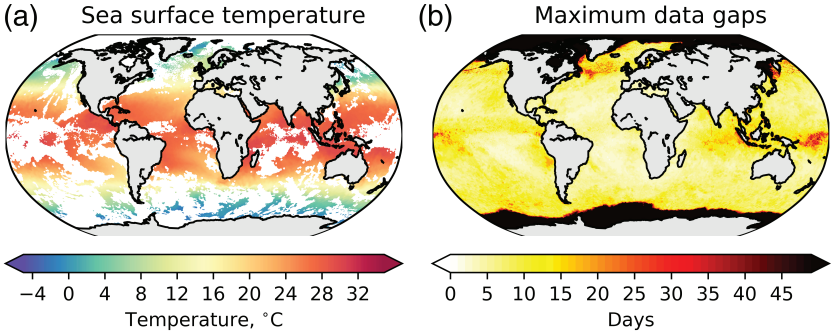


**FIGURE 1** (a) The interpolated SST observations on January 1, 2016. The white part represents the area where no satellite observation is available due to cloud cover. (b) The maximum number of days for which a grid point is not observed

year 2016 using the same configuration as for the later ensemble assimilation run. This simulation was initialized using the state of the last day from the spin-up run. The model state at every fifth day was stored, which resulted in 73 model snapshots in total. From each of these states a running mean over 30 days was subtracted and stored in a matrix so that each column represented a corresponding snapshot. Then a singular value decomposition was computed for this matrix to produce 72 singular values and corresponding singular vectors. The 45 leading singular values and vectors were used to generate the ensemble perturbations using second-order exact sampling. These were added to the state of the last day from the spin-up run to generate the initial ensemble for the data assimilation experiments. Using this method, the initial model uncertainties among different ensemble members were estimated from the temporal variability relative to the running mean during the simulation year. For the atmosphere component, the deterministic initial state from the spin-up run was used for all ensemble states.

## 3.3 | Observation dataset

The assimilated observations are satellite sea-surface temperature (SST) and profile data of temperature and salinity. The satellite SST observations are the Level-3 multi-sensor product (SST_GLO_SST_L3_NRT_OBSERVATIONS_010_010) from the European Union Copernicus Marine Service. The observations are available daily between 80°N and 80°S with a resolution of 0.1°. The unstructured model grid used here is in many regions coarser than the observation grid, while in refined regions it approaches the resolution of the observations. To take this varying resolution into account, super-observations have been generated by averaging the observations within half the model grid resolution around each model grid point. This approach yields a set of super-observations on the model grid. Figure 1a shows the interpolated SST field for January 1, 2016. Figure 1b shows the maximum number of days for which a grid point is not observed during the year 2016. In most regions the maximum duration without observation is below 10 days. Only at high latitudes are there gaps of more than 50 days, which are frequently caused by sea ice. In the equatorial Pacific and Indian Oceans and in the North Atlantic drift region, clouds cause gaps of up to about 30 days, which reduces the influence of the data assimilation in these regions.

The temperature and salinity profiles are provided by the EN4 dataset (EN4.2.1) of the UK Met Office (Good *et al.*, 2013). Compared to the SST data, the profile dataset has a relatively sparse horizontal distribution, while the observations have a much higher resolution in the vertical. Figure 2 shows the location of profile observations of temperature and salinity for all the depths on January 1, 2016. In vertical direction these profiles can reach down to 5,000 m and about 1,000 quality-checked profiles are available each day. In the vertical the observations were interpolated to the layers in FESOM. In the horizontal direction, the observation operator horizontally interpolates the model state onto the observation locations during the data assimilation process.

## 3.4 | Data assimilation experiments

The data assimilation is performed daily for the full year 2016. An ensemble size of 46 is selected to balance the assimilation performance and the computation cost, as with this size we get sufficiently good assimilation behaviour. The standard deviations of the observation errors are set to 0.8°C for the SST, 0.5°C for the profile temperature and 0.5 practical salinity units (psu) for the salinity. The localization radius is set to 300 km. In the coupled model run, the ensemble spread is sufficiently large so that no inflation is required.

The initial state of a coupled model can be far away from the real state, which can cause an instability of the system at the beginning of the assimilation process (Mulholland *et al.*, 2015). Figure 3 shows that, in our case, deviations between the initial model state and the SST observations of up to 10°C are present. These large deviations make a particularly careful application of the data assimilation necessary to avoid devastating shocks to

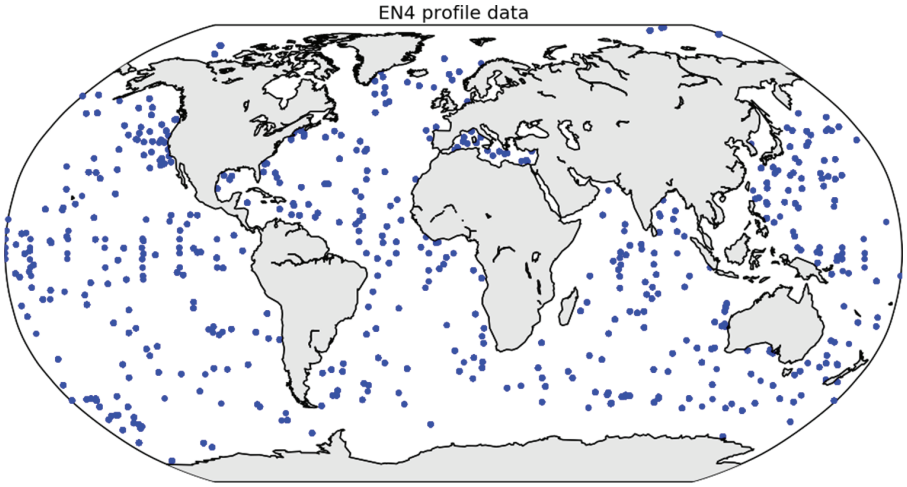


**FIGURE 2** The EN4 quality-checked profile locations on January 1, 2016. Both the temperature and the salinity profile locations are shown

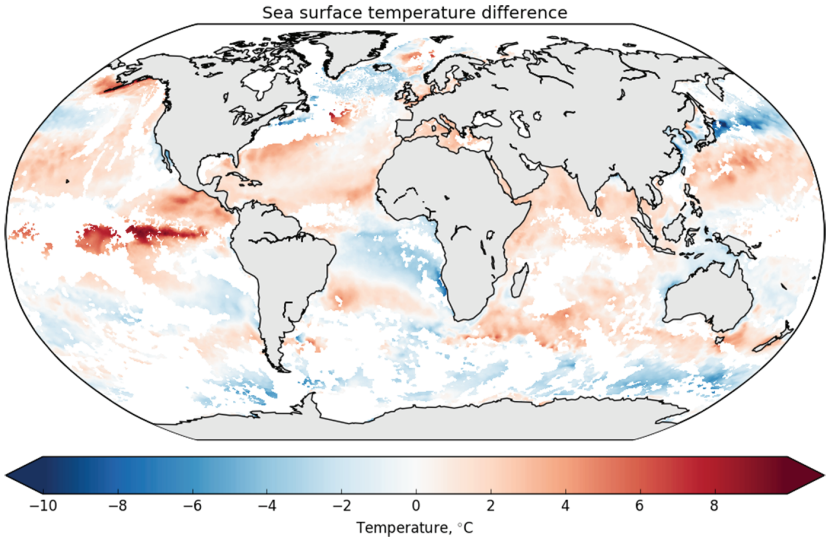


**FIGURE 3** Difference of sea-surface temperature between the observation and the model simulation on January 1, 2016. The highest difference can be up to 10 °C

the model state (Karspeck *et al.*, 2013). To stabilize the data assimilation process we omit extreme SST observations with twice of the observation error. This exclusion avoids too large increments to the model states during the analysis step. This method leads to an omission of about 40% of the observations at the first analysis step. The fraction of omitted observations decreases over time and is below 5% after 80 days.

The second stabilization method is to implement a treatment for SST data at the sea ice edge. The implementation considers the fact that the satellite SST can have points with data, which indicates ice-free conditions, while the model has sea ice. At these places the difference between the observed and the modelled SST provides no valuable information. Accordingly, observations close to model grid points with sea ice are omitted. Further, no assimilation updates are performed for model grid points with sea ice. Without this adaption the assimilation resulted in unphysically low SST under the sea ice close to the sea ice edge.

Four different simulation scenarios were carried out for different types of observations:

1. A free run scenario without data assimilation, denoted as "Free_run";
2. A scenario where only the SST data were assimilated, denoted as "DA_SST";
3. A scenario where only the profile data were assimilated, denoted as "DA_proTS";
4. A scenario where both the SST and profile data were assimilated, denoted as "DA_all".

An overview of all the simulation scenarios is provided in Table 1.

## 3.5 | Performance measures

The root-mean-square error (RMSE) is used to measure the model performance for different simulation scenarios

**TABLE 1** Simulation scenarios with different assimilated observations

| Simulation scenario | Assimilate SST | Assimilate T profile | Assimilate S profile |
|---|---|---|---|
| Free_run | N | N | N |
| DA_SST | Y | N | N |
| DA_proTS | N | Y | Y |
| DA_all | Y | Y | Y |

for different variables:

$$RMSE(X) = \sqrt{\frac{\sum_{i=1}^{n_t}\sum_{j=1}^{n_{nodes\_obs}}[(\overline{X}_{i,j}^{\mathrm{f}} - \overline{X}_{i,j}^{\mathrm{obs}})a_j]^2}{\sum_{i=1}^{n_t}\sum_{j=1}^{n_{nodes\_obs}} a_j{}^2}}$$

where $X$ can be the sea-surface temperature, subsurface temperature, subsurface salinity, 2 m air temperature, or surface pressure; $n_t$ is the number of analysis steps, $n_{nodes\_obs}$ the total number of observations at an analysis step; $a_j$ is the area of the grid cell $j$. The overbar indicates ensemble mean, the superscript f indicates the 1-day forecast corresponding to Kalman Filter update cycles and the superscript obs the daily observations. In our case $n_t$ is the number of days from 1 March to 31 December of year 2016. In the following sections "10-month average" refers to the average over this period. The first 2 months are excluded from the evaluation since they are considered as the initial DA transition time. The area-weighting accounts for the varying resolution of the FESOM mesh.

## 4 | RESULTS AND DISCUSSION

### 4.1 | Impact on the ocean

The RMSE is calculated for the SST, and subsurface temperature and salinity, over all the observation points and the months March to December to evaluate the data assimilation experiments. An overview of the RMSE for the different simulation scenarios is given in Figure 4. Below, we discuss the effect on the different variables.

#### 4.1.1 | Temperature

When assimilating SST in DA_SST, the RMSE of SST is reduced globally by 66% compared to the free run. If only the subsurface temperature and salinity are assimilated (DA_proTS), the reduction of the RMSE of SST is still 47%. This indicates that the limited subsurface temperature information can also improve the SST, utilizing

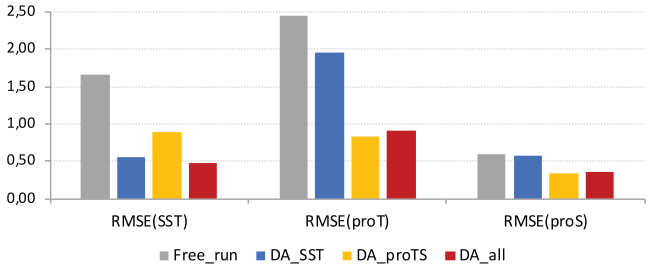


**FIGURE 4** RMSE of SST, subsurface temperature and salinity for different simulation scenarios over months March to December

the high vertical correlations in the mixed layer. Figure 5 shows the 10-month average SST difference between the model simulation and the observations. The difference is strongly decreased in all assimilation scenarios. The global area-weighted 10-month average over the absolute SST difference

$$\mathrm{abs}(SST_{\mathrm{diff}}) = \frac{\sum_{i=1}^{n_t}\sum_{j=1}^{n_{nodes\_obs}}|(\overline{X}_{i,j}^{\mathrm{f}} - \overline{X}_{i,j}^{\mathrm{obs}})a_j|}{\sum_{i=1}^{n_t}\sum_{j=1}^{n_{nodes\_obs}} a_j}$$

is only 0.33°C for the scenario DA_SST and 0.31°C for DA_all. If only profile data are assimilated (DA_proTS), the difference is higher with 0.7°C, which is still only half the difference of 1.41°C in the free run.

The RMSE of the subsurface (full water column as sampled by the profile data) temperature, computed relative to the profile data up to 5,000 m depth, is reduced by 20% (Figure 4, middle) when assimilating only the SST observations (DA_SST). As expected, this influence is larger when assimilating profile data. The reduction reaches 65% in scenario DA_proTS.

Figure 6 shows global area-weighted 10-month average profiles of temperature and salinity and their RMSE and bias between 10 and 230 m depth. In this figure we only account for profiles which hold data for all 15 model layers in this depth range. In Figure 6a, at 10 m depth the RMSE of temperature for the free run is 1.5°C while for DA_SST it is reduced to 0.7°C. The free run as well as DA_SST shows a strongly increasing RMSE of temperature with depth from 10 to 160 m, and a decrease of RMSE below this depth. Assimilating SST only (DA_SST) gives a rather homogeneous reduction of the RMSE for each layer down to 160 m compared to the free run. The effect of DA is still visible at 190 m depth, which shows that the temperature at this depth is correlated to the surface temperature. Assimilating profile data yields overall smaller RMSEs and a maximum reduction of the RMSE of 79% at 160 m depth. At 230 m depth, the RMSE is reduced by 46%. In Figure 6b, the free run shows negative bias for all depths and the bias

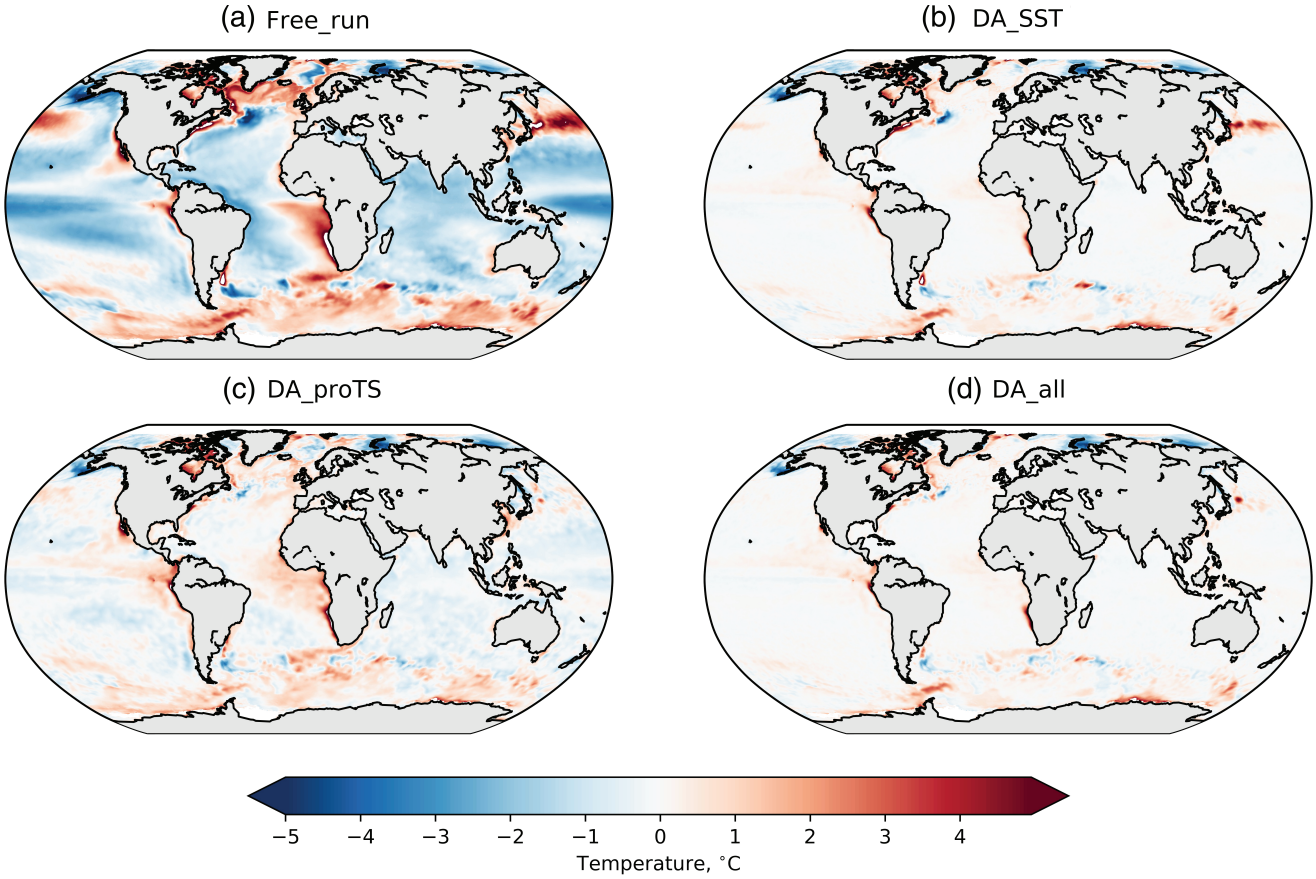


**FIGURE 5** Average difference of sea-surface temperature between the model simulation and the observations over months March to December for different simulation scenarios: (a) Free_run, (b) DA_SST, (c) DA_proTS, and (d) DA_all

becomes stronger with depth with a maximum at 160 m. In DA_SST the bias is largely corrected down to 50 m depth. From 50 to 200 m the correction decreases gradually. Assimilating the profiles yields almost zero bias down to 160 m depth, while from 160 to 230 m the bias is about −0.5°C, which is still small compared to the free run.

The above results show that DA_SST also improves the subsurface temperature, and DA_proTS shows improvements of SST. These effects are caused by the vertical correlations in the ocean induced by the model dynamics.

### 4.1.2 | Salinity

Assimilating the profile observations in scenario DA_proTS leads to a 43% reduction in the RMSE of the subsurface salinity compared to the free run (Figure 4), while assimilating all data in DA_all yields an RMSE reduction of 40%. If only SST data is assimilated (DA_SST), the error in the salinity is reduced by only 5%. These results are consistent with the results of data assimilation for an ocean-only model by Vernieres *et al.* (2014). In Figure 6d it is visible that assimilating SST slightly reduces the salinity RMSE in the upper 100 m. If only the profiles are assimilated (DA_proTS), the RMSE at 10 m depth is 0.41 psu and slightly reduces with depth. The effect of DA is still noticeable at 230 m depth for DA_proTS and DA_all. The DA increases the average bias from 10 to 60 m, where the bias is negative for all cases. From 90 to 230 m depth, the bias is positive and slightly smaller for the assimilation runs than for the free run. Note that the sign and amplitude of the bias is influenced by the choice of the profile included in the computation. Here only profiles are used which have observations at all layers between 10 and 230 m depth. When using all subsurface data, the bias is overall negative (around −0.15 psu for DA_proTS and DA_all), but the profiles are not smooth due to the combination of data from various different sources (not shown).

## 4.2 | Impact on the atmosphere

We evaluate the impact of the DA into the ocean on the atmosphere by comparing the atmospheric variables from the model prediction with daily fields from the ERA-Interim atmospheric reanalysis provided by

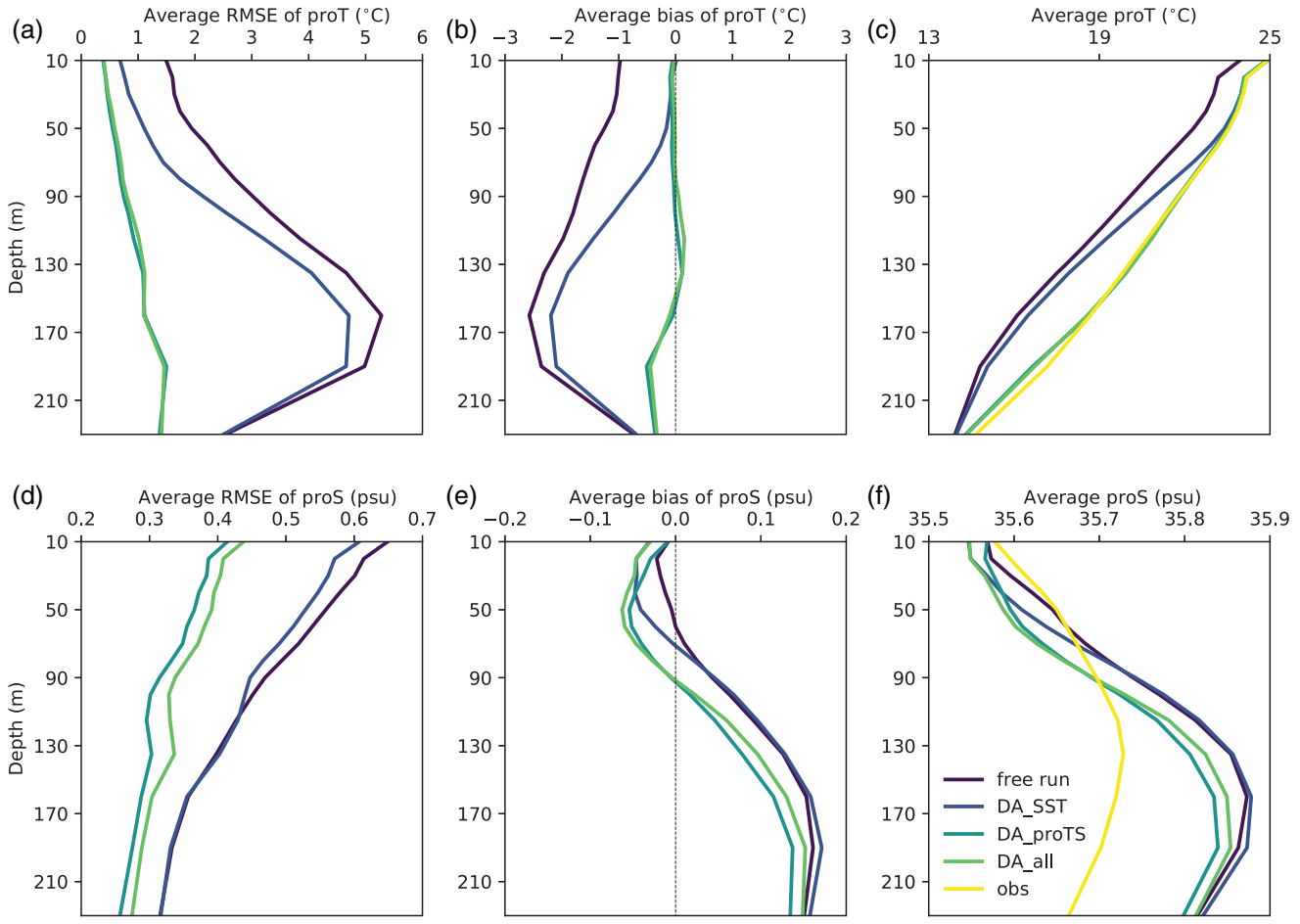


**FIGURE 6** Global average RMSE, bias and the profile value of (a–c) temperature and (d–f) salinity over months March to December as a function of depth

European Centre for Medium-range Weather Forecasts (ECMWF) (Berrisford *et al.*, 2011) for temperature at 2 m above surface, surface pressure, zonal and meridional wind velocity at 10 m above surface. Further, the atmospheric temperature and wind velocity at several pressure levels are examined.

### 4.2.1 | Two-metre temperature

Figure 7 shows the mean difference for the months March to December of temperature at 2 m above the surface between the model simulation and the ERA-Interim reanalysis data for the different simulation scenarios. The free run shows rather large biases of both signs and the average bias is −0.24°C. In general, the three assimilation runs result in an overall more homogeneous and smaller bias. However, a positive bias is visible everywhere over the oceans except in the Arctic Ocean and parts of the Southern Ocean. On average this bias is 0.27°C for DA_SST, 0.27°C for DA_proTS, and 0.24°C for DA_all. When assimilating only profile data in DA_proTS, the spatial pattern of the 2 m temperature bias is very similar to assimilating only SST or both the SST and profile data. This similarity shows that the overall bias is not caused by a bias in satellite SST data. The exact cause for the overall positive bias is unclear, but it is possibly related to differences between ECHAM and ERA-Interim in how the 2 m temperature is diagnosed from the lowest atmospheric layer and surface temperature based on atmospheric conditions.

As SST is at the interface of the ocean and the atmosphere, an improved prediction of SST is expected to lead to a better prediction of the temperature in the atmosphere. However, the effect is only direct for the air temperature above the ocean. Over the continents the changes in the 2 m temperature are less evident than over the ocean. Here, the land model will react and influence the atmosphere, but a detailed analysis of the reaction of the land model is beyond the scope of this study. In general, the strong negative bias over South America is reduced by the assimilation. Likewise, the negative bias over India and Southeast Asia is reduced. On the other hand, the positive bias extending from the eastern Mediterranean to Siberia is increased.

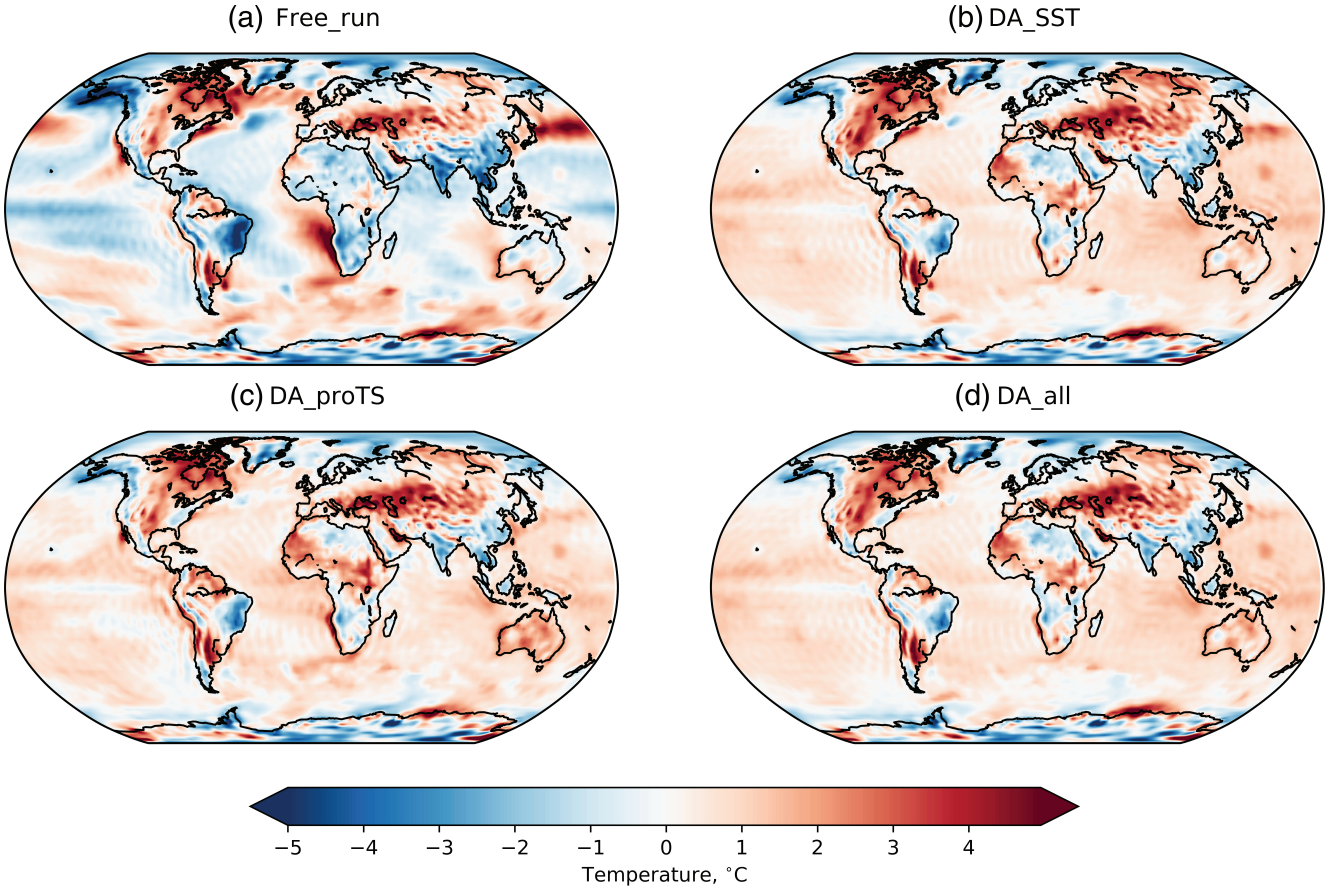


**FIGURE 7** Average bias (model – ERA-Interim) of temperature at 2 m above surface over months March to December for different simulation scenarios: (a) the free run, (b) DA_SST, (c) DA_proTS, and (d) DA_all

### 4.2.2 | Ten-metre wind velocities

The 10-month average bias (model simulation minus ERA-Interim) of the wind velocity field and the wind strength at 10 m above the surface is shown in Figure 8. In the free run, the velocity magnitude at the Equator is overestimated in the Pacific Ocean and underestimated in the Atlantic Ocean. The data assimilation strongly reduces these large differences (by 21.4% in the region from 10°S to 10°N for DA_SST), but the overall flow pattern is maintained. In addition, the bias of wind strength is reduced in the South and North Pacific. In the southern Indian Ocean, the bias is slightly increased due to an eastward flow induced by the DA. The effects are very similar for all assimilation scenarios, but slightly smaller in DA_proTS.

Over land, the 10 m wind velocities in the free run and the three data assimilation runs are rather similar. The assimilation does not give rise to significant influence on the velocities there.

Compared to other weakly-coupled data assimilation studies who assimilate both the ocean and atmosphere observations (e.g. Lea *et al.*, 2015) and thus get an improved atmospheric state, the assimilation into only the ocean component has significant effects on the atmosphere. However, these effects concentrate on the atmosphere above the ocean but not above the land, which is mostly due to the much stronger land influence on the *in situ* atmosphere compared to the remote ocean influence.

### 4.2.3 | Temperature and winds in the free atmosphere

Above we investigated the effect of the ocean DA onto the atmosphere close to the ocean surface. Here, we extend the assessment to the free atmosphere. Figure 9 shows the RMSE of temperature at the pressure levels 925, 850, 500 and 300 hPa for the free run and the experiment DA_all. The other DA scenarios result in overall similar effect, so they are not shown in the figure but the RMSE values for all the scenarios averaged over all the model grids are given in Table 2. At 300 hPa, a particularly large RMSE of up to 5°C is visible in the free run (Figure 9a). This RMSE is strongly reduced to around 1°C by the assimilation. In the high

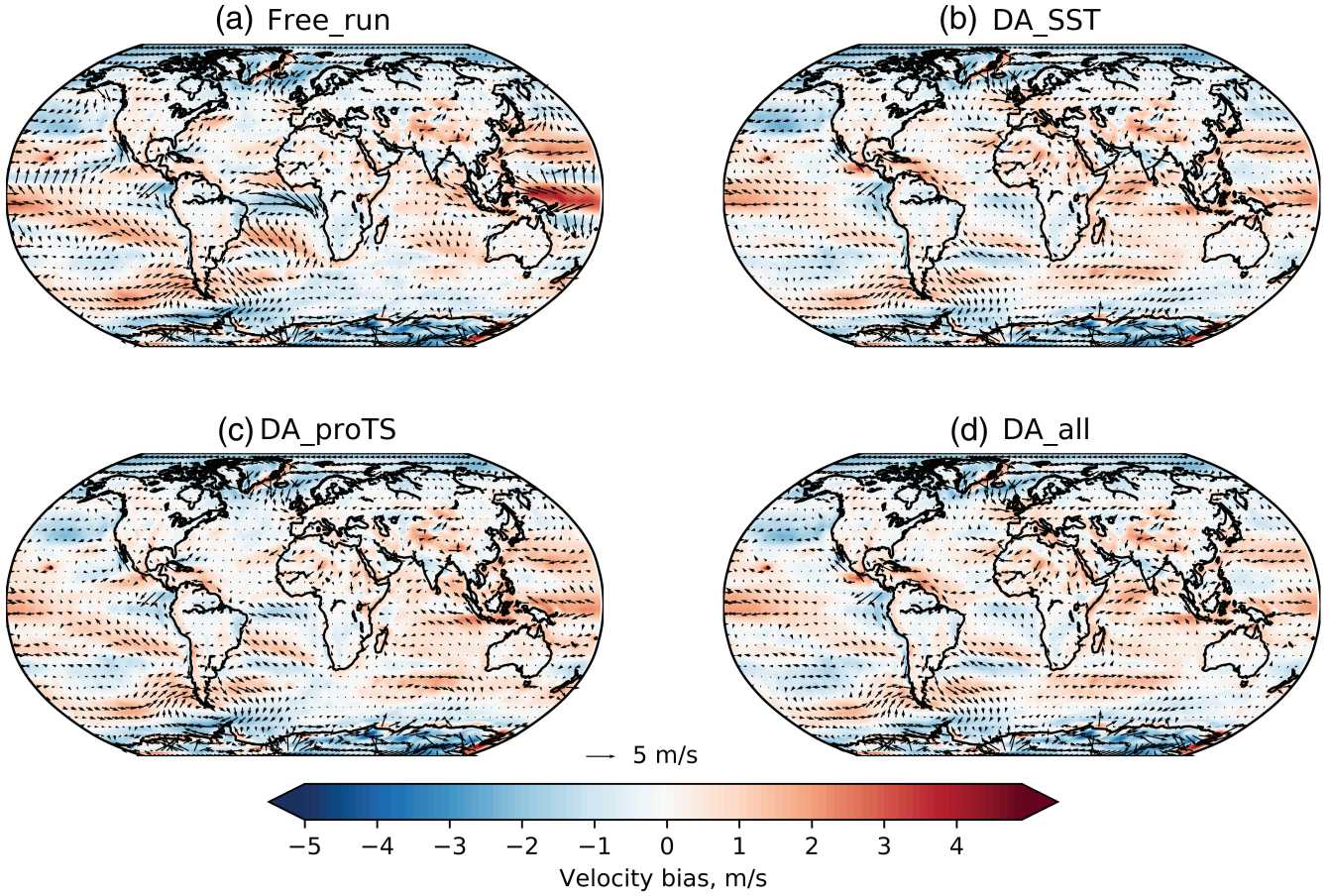


**FIGURE 8** Average bias of wind velocity and wind speed ($m \cdot s^{-1}$) at 10 m above surface over months March to December for different simulation scenarios: (a) the free run, (b) DA_SST, (c) DA_proTS, and (d) DA_all

latitudes, the RMSE remains larger, but is still reduced. At the other pressure levels, the RMSEs are overall lower than at 300 hPA. However, also at these layers, the DA reduces the RMSE. An exception is visible in the eastern Pacific at 925 and 850 hPa, where the RMSE is partly increased by the DA.

Figure 10 shows the bias of the wind field and wind speed at the four pressure levels in the free atmosphere. At 925 hPa, the biases are very similar to those for wind at 10 m (Figure 8). The assimilation reduced biases in the equatorial region, but induced an eastward flow in the southern Indian Ocean. This eastward flow is visible with different strengths at all levels. Overall, the bias amplitudes increase with height, but effects like the reduction of bias in the tropical Atlantic and Pacific Oceans are visible at all levels up to 500 hPa. However, at 850 hPa and higher up in the atmosphere, the DA includes an increased bias over the North Atlantic and Europe as well as a stronger negative bias over the North Pacific. At 300 hPa, also an increased equatorial bias is induced in the Atlantic sector, thus the effect is reversed from the bias reduction at the lower levels.

### 4.2.4 | Physical interpretation of the atmospheric response

For the physical interpretation of the assimilation effect in the atmosphere we focus on some regions where the effect of the assimilation can be well interpreted. Generally, the effects of the corrected SST on atmospheric circulation and clouds are more straightforward in the tropics and subtropics where direct thermal circulations are more pronounced and synoptic variability is weaker compared to the extratropics.

In the free run in the tropical Pacific the SST (Figure 5a) and the 2 m temperature in the atmosphere (Figure 7a) are too low. The bias in the equatorial SST is likely at least partly related to a too-low ocean resolution because tropical instability waves are not resolved (Rackow *et al.*, 2018). This is also consistent with Coupled Model Intercomparison Project (CMIP6) simulation results with the AWI-CM (Semmler *et al.*, 2019). The equatorial cold bias results in a weaker intertropical convergence zone. This is consistent with a divergence bias in the wind which is particularly strong in the western tropical Pacific. The bias is visible in

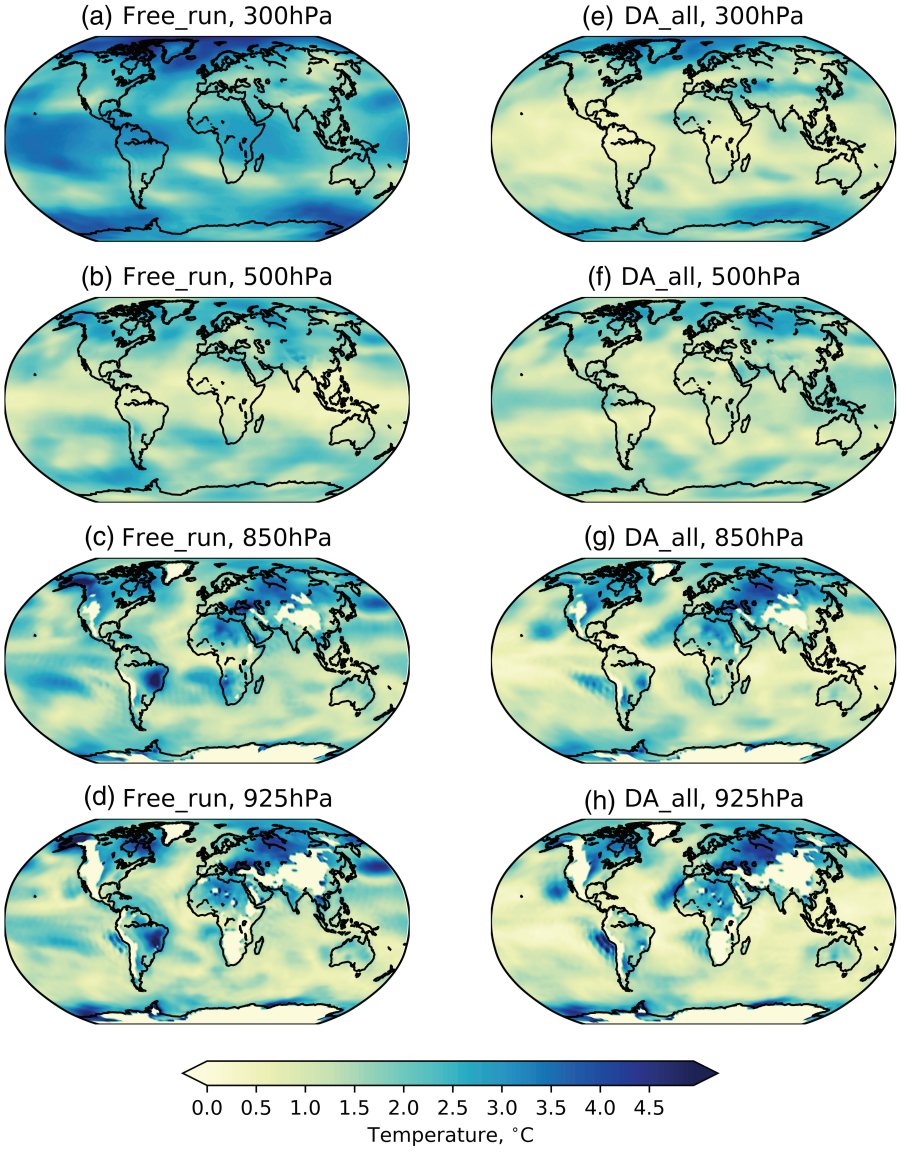


**FIGURE 9** Average RMSE over months March to December of temperature at four pressure levels in the free atmosphere: (a–d) free run; (e–h) assimilation scenario DA_all, results in overall reduced RMSEs

the 10 m winds (Figure 8a), but also at 925 and 850 hPa (Figure 10c,d). The DA corrects the SST in all three DA experiments. The atmosphere reacts on this with a warming (Figure 7) and a significant reduction of the divergence bias in the winds at 850 and 925 hPa (Figure 10g,h) and at 10 m above the ocean (Figure 8b–d). The enhanced equatorial convergence is associated with stronger equatorial ascending motion and convection. Correspondingly, precipitation is enhanced in the western equatorial Pacific and reduced in the adjacent subtropics, reducing a bias pattern of opposite sign in the free run (Figure S1).

Tropical SSTs and thus near-surface temperatures in the free run are colder than observed not only in the equatorial Pacific, but throughout most of the tropics and subtropics (Figures 5 and 7), with some exceptions (see below). The counteracting warming introduced by the DA leads to an even stronger warming in the upper tropical troposphere (Figure S2) due to enhanced convection and

**TABLE 2** RMSE of temperature and wind speed at four levels in the free atmosphere averaged over months March to December for the different simulation scenarios

| Temperature (°C) | Free_run | DA_SST | DA_proTS | DA_all |
|---|---|---|---|---|
| 300 hPa | 2.75 | 1.86 | 1.82 | 1.78 |
| 500 hPa | 1.72 | 1.61 | 1.57 | 1.56 |
| 850 hPa | 2.02 | 1.82 | 1.80 | 1.76 |
| 925 hPa | 2.07 | 1.91 | 1.88 | 1.85 |
| Wind speed ($m \cdot s^{-1}$) | | | | |
| 300 hPa | 5.39 | 5.13 | 4.85 | 5.03 |
| 500 hPa | 3.93 | 3.67 | 3.61 | 3.63 |
| 850 hPa | 2.68 | 2.49 | 2.47 | 2.47 |
| 925 hPa | 2.62 | 2.43 | 2.42 | 2.41 |

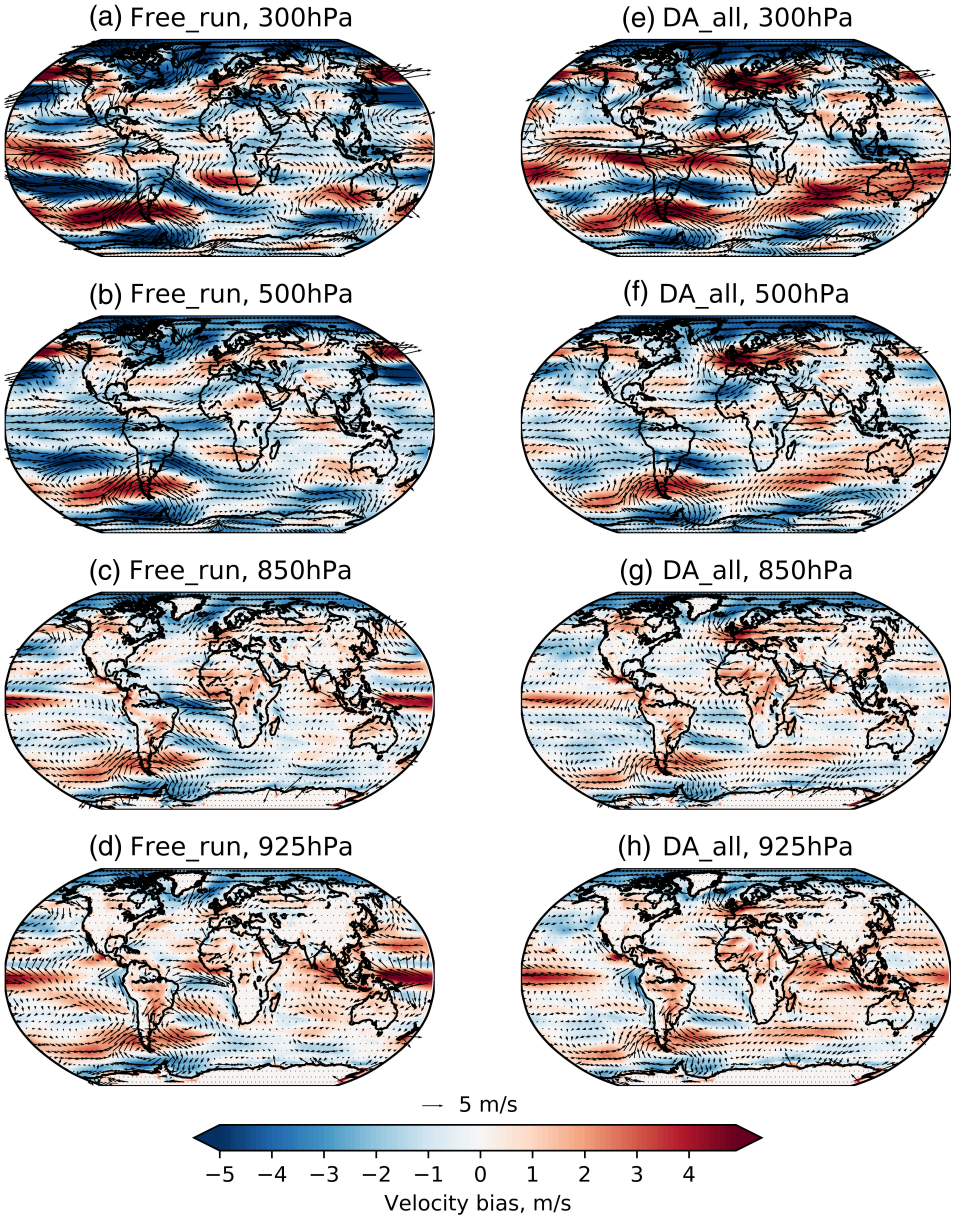


**FIGURE 10** Average bias over months March to December of wind velocity and wind speed ($m \cdot s^{-1}$) at four pressure levels in the free atmosphere: (a–d) free run; (e–h) assimilation scenario DA_all [Colour figure can be viewed at wileyonlinelibrary.com]

the temperature dependence of the moist adiabatic lapse rate (lapse-rate feedback). In fact, the free run exhibits a similar temperature bias pattern of opposite sign, with a significant cold bias in the upper tropical troposphere (300 hPa) of around 4°C (Figure S2a), so that the SST correction results in the largest bias reduction (Figure S2e) and RMSE reduction (Figure 9) in the upper troposphere.

The free run exhibits a cold bias of similar magnitude (~3°C) in the upper troposphere also in the high latitudes (Figure S2a). By correcting the cold bias only in the tropics but not in the high latitudes, the assimilation introduces a too strong Equator-to-Pole temperature gradient particularly in the upper troposphere and thus stronger westerlies over a broad range of latitudes, encompassing the latitudes of the subtropical and polar jets (20–70°N). The remaining heterogeneity in the wind velocity differences between the assimilation runs and ERA-Interim, with some difference wind vectors still pointing eastward (Figure 10), might be due to a low signal-to-noise ratio associated with the short 10-month period considered.

Another effect of the assimilation is visible in the Atlantic to the west of South Africa. Here the SST (Figure 5a) and the 2 m atmospheric temperature in the free run (Figure 7a) show a strong warm bias. In addition, there is a significant wind bias (Figure 8a) and a cloudiness low bias (Figure S3). The westerly wind bias is a common feature of global climate models leading to an SST warm bias and then intensifying the SST warm bias due to reduced ocean upwelling (Bjerkness feedback, see for example Eichhorn and Bader (2017), Voldoire *et al.* (2019)). Furthermore, a lack of stratocumulus clouds commonly exists which intensifies the SST warm bias and

in turn leads to unstable situations and less favorable conditions for stratocumulus cloud formation – another positive feedback loop (Voldoire *et al.*, 2014). The DA reduces the SST bias and also the cloud bias as shown in Figure S3. The cooler SST west of South Africa leads to cooling of the atmosphere and therefore more favorable conditions for cloud formation, and the circulation bias at 10 m in the Atlantic west of South Africa is also strongly reduced (Figure 8b–d).

In the equatorial Atlantic the free run exhibits a cold bias in the east, west of Central Africa, and a warm bias in the west, east of South and Central America, accompanied by a weakened Atlantic Walker Circulation (Figure 8a). The DA largely corrects the zonal temperature gradient (Figure 5) and thereby also the Walker Circulation and cloud distribution (Figures 8b–d and S3b–d).

Apart from the general enhancement of the westerlies in the upper troposphere resulting from the enhanced Equator-to-Pole temperature gradient, the influence of the SST correction on the atmosphere is less clear in the extratropics. For example, the correction of SST differences in the North Pacific, with a pattern similar to the Pacific Decadal Oscillation (e.g. Deser *et al.*, 2010), has only a minor influence on the mean atmospheric circulation there (Figure 8). Continental near-surface air temperature differences, with too-low temperature over Alaska and too-high temperature over northeast America (similar to the Pacific–North American pattern; e.g. Wallace and Gutzler, 1981), are not much influenced either.

## 5 | CONCLUSION

In this work, we investigated the effect of assimilating different types of ocean observations into the ocean component of a coupled ocean–atmosphere model on the fields of the ocean and the atmosphere. The Alfred-Wegener-Institute climate model (AWI-CM) was used as the coupled model to simulate the ocean as well as the atmosphere. Satellite sea-surface temperature and subsurface temperature and salinity profile data were assimilated. The ocean variables sea-surface height, ocean temperature, salinity and velocities were directly updated within this weakly coupled data assimilation system, while the atmosphere only reacted dynamically to the changed ocean state. The data assimilation experiments are evaluated by comparing the predicted sea-surface temperature, subsurface temperature and salinity in the ocean component with ocean observation data. Further, the predicted atmosphere temperature and wind field were compared with reanalysis data from ERA-Interim. In general, the data assimilation improves both the ocean and atmosphere. From the analysis in Section 4, we conclude:

1. The assimilation of sea-surface temperature improved the prediction of both sea-surface temperature and the subsurface ocean temperature. The assimilation of subsurface temperature and salinity data improved the prediction of subsurface ocean temperature and salinity, but also the sea-surface temperature. Assimilating only sea-surface temperature has only a marginal, but positive effect on subsurface salinity. Only if the salinity profiles were assimilated, was the improvement of subsurface salinity significant. These findings are consistent with data assimilation studies using uncoupled ocean models.
2. All assimilation scenarios (assimilating only sea-surface temperature or only the profile or both data types into the ocean component) lead to improvements of the 2 m temperature and the 10 m wind velocity for the atmosphere. While changes in 2 m temperature over the ocean result directly through strong thermal coupling with the ocean, the wind response results from the model dynamics in the coupled ocean–atmosphere model. Improvements tend to be larger in the tropics and over the ocean, whereas effects over land are mostly very small. Assimilating different types of observations gives similar simulation results for the atmosphere, which is expected from similar effects of the assimilation on the ocean surface.
3. The assimilation scenarios also improved the temperature distribution in the free atmosphere, in particular in the tropics where temperature changes are amplified with height due to the temperature dependence of the moist adiabatic lapse rate. Due to a remaining cold bias in the high-latitude upper troposphere (around 300 hPa), an enhanced Equator-to-Pole gradient results in overall too strong westerlies. At lower heights (925 and 850 hPa), however, winds tend to be improved. In the tropical Pacific the correction of a strong sea-surface cold bias leads to an improved representation of the intertropical convection zone with stronger convergence, associated with enhanced ascending motion and convection. In the equatorial Atlantic the assimilation leads to a better representation of the Walker Circulation. We speculate that these improvements in the tropics may act to arrest bias feedback loops between the ocean and the atmosphere which might otherwise act to enhance initial biases in either component.

Overall, the response of the coupled atmosphere to the weakly coupled assimilation of the ocean observations extends through the depth of the troposphere and

has a profound impact on the global atmospheric circulation.

The present weakly coupled data assimilation is limited to assimilating only ocean observations. This directly updates the ocean variables in the assimilation process and has an indirect effect on the atmospheric fields. Obviously, the additional assimilation of atmospheric observations would lead to a direct effect on the atmosphere. The alternative to weakly coupled DA is strongly coupled DA, in which the atmospheric as well as the oceanic variables are updated jointly using cross-covariances between the two components. By now, there are only a few studies applying strongly coupled data assimilation (Lu *et al.*, 2015; Frolov *et al.*, 2016; Sluka *et al.*, 2016). These studies show clearly the benefits of strongly coupled data assimilation, e.g. the ocean analysis errors are reduced compared to the weakly coupled data assimilation in idealized model experiments (Sluka *et al.*, 2016). Given that the data assimilation system used here can be extended to strongly coupled assimilation, this study is a step toward the future investigation of the role of assimilating ocean observations into both the ocean and the atmosphere using a strongly coupled data assimilation system.

## ACKNOWLEDGEMENTS

The work described in this article has received funding from the Initiative and Networking Fund of the Helmholtz Association through the project "ESM – Advanced Earth System Modelling Capacity". LM and HG acknowledge the financial support by the Federal Ministry of Education and Research of Germany in the framework of the research group Seamless Sea Ice Prediction (SSIP; Grant 01LN1701A). The authors acknowledge the North-German Supercomputing Alliance (HLRN) for providing HPC resources in the project hbk00064 and the Earth System Modelling Project (ESM) for funding this work by providing computing time on the ESM partition of the supercomputer JUWELS at the Jülich Supercomputing Centre (JSC). We thank the editors and reviewers for reviewing this article and their comments and suggestions provide useful information for the improvement of our article. Open access funding enabled and organized by Projekt DEAL.

## ORCID

*Qi Tang* https://orcid.org/0000-0002-2109-7935
*Longjiang Mu* https://orcid.org/0000-0001-5668-8025
*Dmitry Sidorenko* https://orcid.org/0000-0001-8579-6068
*Helge Goessling* https://orcid.org/0000-0001-9018-1383
*Tido Semmler* https://orcid.org/0000-0002-2254-4901
*Lars Nerger* https://orcid.org/0000-0002-1908-1010

## REFERENCES

Anderson, J.L. and Anderson, S.L. (1999) A Monte Carlo implementation of the nonlinear filtering problem to produce ensemble assimilations and forecasts. *Monthly Weather Review*, 127, 2741–2758.

Androsov, A., Nerger, L., Schnur, R., Schröter, J., Albertella, A., Rummel, R., Savcenko, R., Bosch, W., Skachko, S. and Danilov, S. (2019) On the assimilation of absolute geodetic dynamic topography in a global ocean model: impact on the deep ocean state. *Journal of Geodesy*, 93, 141–157.

Baehr, J., Fröhlich, K., Botzet, M., Domeisen, D.I.V., Kornblueh, L., Notz, D., Piontek, R., Pohlmann, H., Tietsche, S. and Müller, W.A. (2015) The prediction of surface temperature in the new seasonal prediction system based on the MPI-ESM coupled climate model. *Climate Dynamics*, 44, 2723–2735.

Berrisford, P., Dee, D.P., Poli, P., Brugge, R., Fielding, M., Fuentes, M., Kållberg, P., Kobayashi, S., Uppala, S. and Simmons, A. (2011) *The ERA-Interim archive*, version 2.0. ERA Report Series, pp 23. Reading, UK: ECMWF.

Browne, P.A., De Rosnay, P., Zuo, H., Bennett, A. and Dawson, A. (2019) Weakly coupled ocean–atmosphere data assimilation in the ECMWF NWP system. *Remote Sensing*, 11(3), 234.

Brune, S., Nerger, L. and Baehr, J. (2015) Assimilation of oceanic observations in a global coupled Earth system model with the SEIK filter. *Ocean Modelling*, 96, 254–264.

Chang, Y.-S., Zhang, S., Rosati, A., Delworth, T.L. and Stern, W.F. (2013) An assessment of oceanic variability for 1960–2010 from the GFDL ensemble coupled data assimilation. *Climate Dynamics*, 40, 775–803.

Danilov, S. (2013) Ocean modeling on unstructured meshes. *Ocean Modelling*, 69, 195–210.

Deser, C., Alexander, M.A., Xie, S.-P. and Phillips, A.S. (2010) Sea surface temperature variability: patterns and mechanisms. *Annual Review of Marine Science*, 2, 115–143.

Docquier, D., Grist, J.P., Roberts, M.J., Roberts, C.D., Semmler, T., Ponsoni, L., Massonnet, F., Sidorenko, D., Sein, D.V., Iovino, D., Bellucci, A. and Fichefet, T. (2019) Impact of model resolution on Arctic sea ice and North Atlantic Ocean heat transport. *Climate Dynamics*, 53, 4989–5017.

Eichhorn, A. and Bader, J. (2017) Impact of tropical Atlantic sea-surface temperature biases on the simulated atmospheric circulation and precipitation over the Atlantic region: an ECHAM6 model study. *Climate Dynamics*, 49, 2061–2075.

Evensen, G. (2003) The ensemble Kalman filter: theoretical formulation and practical implementation. *Ocean Dynamics*, 53, 343–367.

Frolov, S., Bishop, C.H., Holt, T., Cummings, J. and Kuhl, D. (2016) Facilitating strongly coupled ocean–atmosphere data assimilation with an interface solver. *Monthly Weather Review*, 144, 3–20.

Goessling, H.F., Tietsche, S., Day, J.J., Hawkins, E. and Jung, T. (2016) Predictability of the Arctic sea ice edge. *Geophysical Research Letters*, 43, 1642–1650.

Good, S.A., Martin, M.J. and Rayner, N.A. (2013) EN4: quality controlled ocean temperature and salinity profiles and monthly objective analyses with uncertainty estimates. *Journal of Geophysical Research: Oceans*, 118, 6704–6716.

Guiavarc'h, C., Roberts-Jones, J., Harris, C., Lea, D.J., Ryan, A. and Ascione, I. (2019) Assessment of ocean analysis and forecast from an atmosphere–ocean coupled data assimilation operational system. *Ocean Science*, 15, 1307–1326.

Haarsma, R.J., Roberts, M.J., Vidale, P.L., Senior, C.A., Bellucci, A., Bao, Q., Chang, P., Corti, S., Fučkar, N.S., Guemas, V., Von Hardenberg, J., Hazeleger, W., Kodama, C., Koenigk, T., Leung, L.R., Lu, J., Luo, J.J., Mao, J., Mizielinski, M.S., Mizuta, R., Nobre, P., Satoh, M., Scoccimarro, E., Semmler, T., Small, J. and Von Storch, J.S. (2016) High resolution model intercomparison project (HighResMIP v1.0) for CMIP6. *Geoscientific Model Development*, 9, 4185–4208.

Hamill, T.M., Whitaker, J.S. and Snyder, C. (2001) Distance-dependent filtering of background error covariance estimates in an ensemble Kalman filter. *Monthly Weather Review*, 129, 2776–2790.

Houtekamer, P.L. and Mitchell, H.L. (2001) A sequential ensemble Kalman filter for atmospheric data assimilation. *Monthly Weather Review*, 129, 123–137.

Juricke, S., Goessling, H.F. and Jung, T. (2014) Potential sea ice predictability and the role of stochastic sea ice strength perturbations. *Geophysical Research Letters*, 41, 8396–8403.

Karspeck, A.R., Danabasoglu, G., Anderson, J., Karol, S., Collins, N., Vertenstein, M., Raeder, K., Hoar, T., Neale, R., Edwards, J. and Craig, A. (2018) A global coupled ensemble data assimilation system using the Community Earth System Model and the Data Assimilation Research Testbed. *Quarterly Journal of the Royal Meteorological Society*, 144(717), 2404–2430.

Karspeck, A.R., Yeager, S., Danabasoglu, G., Hoar, T., Collins, N., Raeder, K., Anderson, J. and Tribbia, J. (2013) An ensemble adjustment Kalman filter for the CCSM4 ocean component. *Journal of Climate*, 26, 7392–7413.

Kunii, M., Ito, K. and Wada, A. (2017) Preliminary test of a data assimilation system with a regional high-resolution atmosphere–ocean coupled model based on an ensemble Kalman filter. *Monthly Weather Review*, 145, 565–581.

Kurtz, W., He, G., Kollet, S.J., Maxwell, R.M., Vereecken, H. and Franssen, H.-J. (2016) TerrSysMP–PDAF (version 1.0): a modular high-performance data assimilation framework for an integrated land surface–subsurface model. *Geoscientific Model Development*, 9, 1341–1360.

Laloyaux, P., Balmaseda, M., Dee, D., Mogensen, K. and Janssen, P. (2016) A coupled data assimilation system for climate reanalysis. *Quarterly Journal of the Royal Meteorological Society*, 142(694), 65–78.

Large, W.G. and Yeager, S. (2009) The global climatology of an interannually varying air–sea flux data set. *Climate Dynamics*, 33, 341–364.

Lea, D.J., Mirouze, I., Martin, M.J., King, R.R., Hines, A., Walters, D. and Thurlow, M. (2015) Assessing a new coupled data assimilation system based on the Met Office coupled atmosphere–land–ocean–sea ice model. *Monthly Weather Review*, 143, 4678–4694.

Liu, Z., Wu, S., Zhang, S., Liu, Y. and Rong, X. (2013) Ensemble data assimilation in a simple coupled climate model: the role of ocean–atmosphere interaction. *Advances in Atmospheric Sciences*, 30, 1235–1248.

Lu, F., Liu, Z., Zhang, S., Liu, Y. and Jacob, R. (2015) Strongly coupled data assimilation using leading averaged coupled covariance (LACC). Part II: CGCM experiments. *Monthly Weather Review*, 143, 4645–4659.

Miller, A.J., Collins, M., Gualdi, S., Jensen, T.G., Misra, V., Pezzi, L.P., Pierce, D.W., Putrasahan, D., Seo, H. and Tseng, Y.-H. (2017) Coupled ocean–atmosphere modeling and predictions. *Journal of Marine Research*, 75, 361–402.

Mu, L., Yang, Q., Losch, M., Losa, S.N., Ricker, R., Nerger, L. and Liang, X. (2018) Improving sea ice thickness estimates by assimilating CryoSat-2 and SMOS sea ice thickness data simultaneously. *Quarterly Journal of the Royal Meteorological Society*, 144(711), 529–538.

Mulholland, D.P., Laloyaux, P., Haines, K. and Balmaseda, M.A. (2015) Origin and impact of initialization shocks in coupled atmosphere–ocean forecasts. *Monthly Weather Review*, 143, 4631–4644.

Nerger, L. and Hiller, W. (2013) Software for ensemble-based data assimilation systems – implementation strategies and scalability. *Computers and Geosciences*, 55, 110–118.

Nerger, L., Hiller, W. and Schröter, J. (2005) PDAF – the parallel data assimilation framework: experiences with Kalman filtering. In: *Use of High Performance Computing in Meteorology*. Reading, UK: World Scientific, pp. 63–83.

Nerger, L., Janjić, T., Schröter, J. and Hiller, W. (2012a) A regulated localization scheme for ensemble-based Kalman filters. *Quarterly Journal of the Royal Meteorological Society*, 138(664), 802–812.

Nerger, L., Janjić, T., Schröter, J. and Hiller, W. (2012b) A unification of ensemble square root Kalman filters. *Monthly Weather Review*, 140, 2335–2345.

Nerger, L., Tang, Q. and Mu, L. (2019) Efficient ensemble data assimilation for coupled models with the Parallel Data Assimilation Framework: example of AWI-CM. *Geoscientific Model Development Discussion*, 2019, 1–23.

Penny, S.G. and Hamill, T.M. (2017) Coupled data assimilation for integrated Earth system analysis and prediction. *Bulletin of the American Meteorological Society*, 98, 7, ES169–ES172.

Pham, D.T., Verron, J. and Roubaud, M.C. (1998) A singular evolutive extended Kalman filter for data assimilation in oceanography. *Journal of Marine Systems*, 16, 323–340.

Rackow, T., Goessling, H.F., Jung, T., Sidorenko, D., Semmler, T., Barbi, D. and Handorf, D. (2018) Towards multi-resolution global climate modeling with ECHAM6-FESOM. Part II: Climate variability. *Climate Dynamics*, 50, 2369–2394.

Sein, D.V., Koldunov, N.V., Danilov, S., Sidorenko, D., Wekerle, C., Cabos, W., Rackow, T., Scholz, P., Semmler, T., Wang, Q. and Jung, T. (2018) The relative influence of atmospheric and oceanic model resolution on the circulation of the North Atlantic Ocean in a coupled climate model. *Journal of Advances in Modeling Earth Systems*, 10, 2026–2041.

Semmler, T., Danilov, S., Gierz, P., Goessling, H., Hegewald, J., Hinrichs, C., Koldunov, N.V., Khosravi, N., Mu, L. and Rackow, T. (2019) Simulations for CMIP6 with the AWI climate model AWI-CM-1-1. https://doi.org/10.1002/essoar.10501538.2.

Semmler, T., Stulic, L., Jung, T., Tilinina, N., Campos, C., Gulev, S. and Koracin, D. (2016) Seasonal atmospheric responses to reduced Arctic sea ice in an ensemble of coupled model simulations. *Journal of Climate*, 29, 5893–5913.

Sidorenko, D., Rackow, T., Jung, T., Semmler, T., Barbi, D., Danilov, S., Dethloff, K., Dorn, W., Fieg, K. and Goessling, H.F. (2015) Towards multi-resolution global climate modeling with ECHAM6–FESOM. Part I: Model formulation and mean climate. *Climate Dynamics*, 44, 757–780.

Skachko, S., Buehner, M., Laroche, S., Lapalme, E., Smith, G., Roy, F., Surcel-Colan, D., Bélanger, J.M. and Garand, L. (2019) Weakly coupled atmosphere–ocean data assimilation in the Canadian

global prediction system (v1). *Geoscientific Model Development*, 12, 5097–5112.

Sluka, T.C., Penny, S.G., Kalnay, E. and Miyoshi, T. (2016) Assimilating atmospheric observations into the ocean using strongly coupled ensemble data assimilation. *Geophysical Research Letters*, 43, 752–759.

Stevens, B., Giorgetta, M., Esch, M., Mauritsen, T., Crueger, T., Rast, S., Salzmann, M., Schmidt, H., Bader, J., Block, K., Brokopf, R., Fast, I., Kinne, S., Kornblueh, L., Lohmann, U., Pincus, R., Reichler, T. and Roeckner, E. (2013) Atmospheric component of the MPI-M Earth system model: ECHAM6. *Journal of Advances in Modeling Earth Systems*, 5, 146–172.

Sugiura, N., Awaji, T., Masuda, S., Mochizuki, T., Toyoda, T., Miyama, T., Igarashi, H. and Ishikawa, Y. (2008) Development of a four-dimensional variational coupled data assimilation system for enhanced analysis and prediction of seasonal to interannual climate variations. *Journal of Geophysical Research: Oceans*, 113, C10017. https://doi.org/10.1029/2008JC004741.

Valcke, S., Craig, T. and Coquart, L. (2013) OASIS3-MCT User Guide, OASIS3-MCT 2.0. Toulouse, France: CERFACS/CNRS SUC URA 1875.

Vernieres, G., Kovach, R., Keppenne, C., Akella, S., Brucker, L. and Dinnat, E. (2014) The impact of the assimilation of Aquarius sea surface salinity data in the GEOS ocean data assimilation system. *Journal of Geophysical Research: Oceans*, 119, 6974–6987.

Voigt, A. and Shaw, T.A. (2016) Impact of regional atmospheric cloud radiative changes on shifts of the extratropical jet stream in response to global warming. *Journal of Climate*, 29, 8399–8421.

Voldoire, A., Claudon, M., Caniaux, G., Giordani, H. and Roehrig, R. (2014) Are atmospheric biases responsible for the tropical Atlantic SST biases in the CNRM-CM5 coupled model? *Climate Dynamics*, 43, 2963–2984.

Voldoire, A., Exarchou, E., Sanchez-Gomez, E., Demissie, T., Deppenmeier, A.-L., Frauen, C., Goubanova, K., Hazeleger, W., Keenlyside, N., Koseki, S., Prodhomme, C., Shonk, J., Toniazzo, T. and Traoré, A.-K. (2019) Role of wind stress in driving SST biases in the tropical Atlantic. *Climate Dynamics*, 53, 3481–3504.

Wallace, J.M. and Gutzler, D.S. (1981) Teleconnections in the geopotential height field during the Northern Hemisphere winter. *Monthly Weather Review*, 109, 784–812.

Wang, Q., Danilov, S., Sidorenko, D., Timmermann, R., Wekerle, C., Wang, X., Jung, T. and Schröter, J. (2014) The Finite Element Sea ice–Ocean Model (FESOM) v.1.4: formulation of an ocean general circulation model. *Geoscientific Model Development*, 7, 663–693.

Yang, Q., Losa, S.N., Losch, M., Liu, J., Zhang, Z., Nerger, L. and Yang, H. (2015) Assimilating summer sea-ice concentration into a coupled ice–ocean model using a LSEIK filter. *Annals of Glaciology*, 56, 38–44.

Zhang, S., Harrison, M.J., Rosati, A. and Wittenberg, A. (2007) System design and evaluation of coupled ensemble data assimilation for global oceanic climate studies. *Monthly Weather Review*, 135, 3541–3564.

## SUPPORTING INFORMATION

Additional supporting information may be found online in the Supporting Information section at the end of this article.

**How to cite this article:** Tang Q, Mu L, Sidorenko D, Goessling H, Semmler T, Nerger L. Improving the ocean and atmosphere in a coupled ocean–atmosphere model by assimilating satellite sea-surface temperature and subsurface profile data. *Q J R Meteorol Soc*. 2020;146:4014–4029. https://doi.org/10.1002/qj.3885